Proceedings of the ASME 2010 3rd Joint US-European Fluids Engineering Summer Meeting and 8th International Conference on Nanochannels, Microchannels, and Minichannels
FEDSM-ICNMM2010
August 1-5, 2010, Montreal, Canada

FEDSM-ICNMM2010-31174

A HYBRID MODEL FOR PREDICTING GAS ENTRAINMENT IN A SMALL BRANCH FROM A CO-CURRENT FLOWING GAS-LIQUID REGIME

Robert Bowden, Wael Saleh, Ibrahim Hassan
Concordia University
Montreal, Quebec, Canada

ABSTRACT

An analytical model was developed to predict the critical conditions at the onset of gas entrainment in a single downward oriented branch. The branch was installed on a horizontal square cross-sectional channel having a smooth stratified co-currently flowing gas-liquid regime in the upstream inlet region. The branch flow was simulated as a three-dimensional point-sink while the downstream run flow was treated with a uniform velocity at the critical dip location. A boundary condition was imposed in the model whereby the flow distribution between the branch and run was obtained experimentally and digital imaging was used to quantify the critical dip location through the dip angle. Three constant dip angles were evaluated in the model and results showed the dip height to have good agreement with experiments between angles of 50 and 60 degrees. The predicted upstream height, however, did not match well with the experimentally determined height due to the omission of shear and inertial effects between the upstream location and critical dip.

INTRODUCTION

Two-phase flow in branching conduits is a widely studied topic with a variety of motivating applications, including oil-gas production and safety analysis in nuclear power plants. Efficient two-phase flow separation can lead to improved performance of oil-gas production plants [1], and has been investigated experimentally [2] and analytically [3].

In normally single fluid phase systems, prior knowledge of two-phase operating conditions are important for predicting accident scenarios [4, 5]. Single and multi-junction configurations have been studied for this purpose, focusing on either the critical conditions leading to two-phase flow, or the two-phase flow characteristics. Empirical models derived from these types of experimental programs, for example the horizontal stratification entrainment model, have been used in thermalhydraulic codes for accident analysis [6].

Zuber [7] reviewed the two-phase phenomena at a small branch on the side of a large reservoir containing stratified layers of gas and liquid fluid phases. With single phase liquid initially flowing into the branch, the onset of gas entrainment (OGE) was described by mechanisms that included either vortex induced or vortex-free gas entrainment. The critical liquid height (H_{OGE}) at which vortex-free OGE occurred was found to be a function of the branch flow Froude (Fr_d) number, which is a ratio of the branch fluid inertia to gravity.

A variety of quasi-steady experiments were later conducted with one, two, or three branches on a wall exposed to a large stratified two-phase reservoir [8, 9]. In these studies the critical liquid height was recorded at a stagnant reference point within the large two-phase reservoir. Of these, Saleh et al. [9] used a digital imaging technique to record the OGE dip curvature and produced a semi-empirical model that compensated for the effects of interfacial surface tension at low Froude numbers. The critical heights in these studies were found to significantly differ from measurements conducted in horizontal channels with co-current stratified gas-liquid flows with equivalent branch Froude numbers.

Reimann and Khan [10] investigated the critical height at the onset of vortex-free gas entrainment in a 206 mm internal diameter horizontal pipe with a single downward branch whose diameter ranged between 6, 12, and 20 mm. The liquid height measurements were conducted at a location approximately 0.5 m upstream of the branch. They discussed that the water's velocity in the pipe (0.2 to 0.8 m/s) had negligible influence on the critical height since the branch velocity was significantly larger than the crossflow velocity. This was later corroborated by Smoglie and Reimann [11] who demonstrated that their correlation of the critical height, represented here as,

$$\frac{H_{OGE}}{d} = 1.06 Fr_d^{0.4} \quad (1)$$

was independent of the ratio between the run ($\rho_L V_{L2S}^2$) and branch ($\rho_L V_{L3}^2$) superficial momentum fluxes over the range,

$$0.1 \times 10^{-4} \le \frac{\rho_L V_{L2}^2}{\rho_L V_{L3}^2} \le 40 \times 10^{-4}$$

Maciaszek and Micaelli [12] also experimented with gas entrainment in a downward branch using pipe diameters of 80 and 135 mm and branch diameters of 12 and 20 mm, respectively. Their tests were conducted at operating pressures between 2 and 7 MPa. The authors found that their data was correlated by,

$$\frac{H_{OGE}}{d} = 0.335 Fr_d^{0.4} \quad (2)$$

and argued that the transverse liquid velocity in the pipe (up to 3 m/s) drastically reduced the value of the critical height when compared to Smoglie and Reimann [11]'s correlation in Eq. (1).

The correlations provided by Smoglie and Reimann [11] and Maciaszek and Micaelli [12] provide dramatically different predictions in critical height and flow quality, although the entrainment phenomenon was reportedly quite similar. This led the present authors to recently model the gas entrainment phenomenon under liquid crossflow conditions [13]. The model followed a potential flow approach based on earlier work using semi-infinite stagnant two-phase domains [14]. This earlier model was based on an unconfined geometry – a branch in a semi-infinite medium. This posed a challenge when trying to compare the predictions with finite sized geometries. The present study improves the earlier analysis by modeling the branch within a confined horizontal channel. The authors' recently presented an experimental study of the critical height at the onset of gas entrainment [15]. The study also contains the details of the facility and methodology. Data presented in Hassan et al. [15] were used in this study as empirical boundary conditions, and the relevant data is also presented here for completeness.

NOMENCLATURE

A	point on the interface upstream of the branch
B	lowest point of the dip
a_y	vertical acceleration, (m/s^2)
d	branch diameter, (m)
D	horizontal pipe diameter, (m)
Fr_d	discharge Froude number
Fr_U	crossflow Froude number
g	acceleration due to gravity, (m/s^2)
h	dip height, (m)
$\vec{i}, \vec{j}, \vec{k}$	unit length directional vectors in x, y, z
H	upstream interface height, (m)
H_{OGE}	critical height at onset of gas entrainment, (m)
L	inlet and run pipe length, (m)
m	mass flow rate, (kg/s)
P	pressure, (N/m^2)
Q	volume flow rate, (m^3/s) or (L/min)
u, v, w	velocity components in x, y, z, (m/s)
U	horizontal velocity with uniform profile, (m/s)
V	velocity, (m/s)
V_{L2S}	superficial liquid velocity in the run, (m/s)
V_{L3}	average liquid velocity in the branch, (m/s)
x, y, z	Cartesian coordinate system,

Greek

θ_B	dip angle, (degrees)
λ	x-location where H is measured, (m)
μ	fluid viscosity, (Ns/m^2)
σ	gas-liquid interface surface tension, (N/m)
ρ	fluid density, (kg/m^3)
$\Delta\rho$	density difference of fluid phases, (kg/m^3)
ϕ_B	potential function at dip, (m^2/s)
$\phi_{crossflow}\big\|_B$	crossflow potential function, (m^2/s)
$\phi_{\sin k}$	point-sink potential function, (m^2/s)
$\vec{\nabla}$	gradient operator

Subscripts

d	branch
G	gas phase
L	liquid phase
1, 2, 3	inlet (1), run (2) and branch (3)

THEORETICAL ANALYSIS

A horizontal pipe, having a square cross-section of side length D, is shown in Fig. 1 to have a bottom oriented branch of diameter d. The branch inlet is the origin of the Cartesian coordinate system ($x = 0$, $y = 0$, $z = 0$). Liquid flows into the branch with a mass flow rate of m_{L3}, and flows out of the run with a mass flow rate of m_{L2}. Gas flows out of the run with a mass flow rate of m_{G2}. The interfacial shear induced by the gas phase is neglected in this study. A steady dip forms in the gas-liquid interface, with its lowest point located at B ($x = b$, $y = h$, $z = 0$). Applying Bernoulli's equation on each side of the gas-liquid interface between point A ($x = -\lambda$, $y = H_{OGE}$, $z = 0$) and point B, and summing the two resulting equations, the liquid phase kinetic energy at point B, V_B^2, can be expressed as,

$$V_B^2 = 2g\frac{\Delta\rho}{\rho_L}\left(H_{OGE} - h\right) + V_A^2 \quad (3)$$

The inlet liquid height is denoted as $y_A = H_{OGE}$ while the dip height is $y_B = h$. Assuming that the velocity profile at the inlet is uniform, the interface kinetic energy at point A, V_A^2, can be found using the average velocity, U_A, as,

$$V_A \equiv U_A = \frac{Q_{L2} + Q_{L3}}{H_{OGE} \cdot D} \tag{4}$$

This is found through conservation of mass, as the inlet liquid flow rate is a summation of the run, Q_{L2}, and branch, Q_{L3}, liquid flow rates. The inlet liquid flow area is the product of the channel width, D, by the liquid height, H_{OGE}. Substituting Eq. (4) into Eq. (3) yields,

$$V_B^2 = 2g\frac{\Delta\rho}{\rho_L}\left(H_{OGE} - h\right) + \left(\frac{Q_{L2} + Q_{L3}}{H_{OGE} \cdot D}\right)^2 \tag{5}$$

For any given flow condition (Q_{L2}, Q_{L3}) there are three unknowns in Eq. (5), namely V_B^2, H_{OGE}, and h. Two additional equations are therefore needed to solve for the two remaining unknowns.

The steady vertical acceleration at any point in the flow field can be found from White [16] using the velocity vector components (u, v, w) in the Cartesian coordinate system (x, y, z) through,

$$a_y = u\frac{\partial v}{\partial x} + v\frac{\partial v}{\partial y} + w\frac{\partial v}{\partial z} \tag{6}$$

The criterion to predict the dip instability at the onset of gas entrainment is defined from the vertical acceleration being equivalent to gravity as,

$$a_y\big|_B = -g \tag{7}$$

The gravitational acceleration is given by $-g$ (-9.81 m/s^2), with the negative sign indicating that it is acting in the negative y-direction. Assuming that the velocity field local to the branch can be represented by a superposition of a point-sink in uniform crossflow (x-direction), results in a total potential function, ϕ, described by,

$$\phi = \left(\phi_{crossflow} + \phi_{\sin k}\right) \tag{8}$$

where the velocity components can be found through,

$$\vec{V} = \vec{\nabla}\phi \tag{9}$$

The vertical acceleration at point B can be found through substitution of the velocity field definition in Eq. (9) into Eq. (6), and the onset criterion is found as,

$$a_y\big|_B = \left(\frac{\partial\phi}{\partial x}\frac{\partial^2\phi}{\partial x\,\partial y} + \frac{\partial\phi}{\partial y}\frac{\partial^2\phi}{\partial y^2} + \frac{\partial\phi}{\partial z}\frac{\partial^2\phi}{\partial y\partial z}\right)\Bigg|_{(x=b,\,y=h,\,z=0)} = -g \tag{10}$$

The crossflow velocity at point B is assumed to have a uniform profile, U_B, and independent of the y coordinate. Its magnitude is found as a quotient of the liquid flow rate in the run, Q_{L2}, and liquid flow area beneath the dip, which is a product of the dip height h and channel width D. The resulting potential function is therefore found, following from Schetz and Fuhs [17], as,

$$\phi_{crossflow} = U_B x \tag{11}$$

where,

$$\left.\frac{\partial\phi_{crossflow}}{\partial x}\right|_{x=b,\,y=h,\,z=0} = \frac{Q_{L2}}{hD} \tag{12}$$

at the lowest point of the dip ($x = b$, $y = h$, $z = 0$). The point-sink velocity at point B is found through a quotient of the branch flow rate, Q_{L3}, and the sink flow area, which in this case is simulated as a hemisphere with a radius of $\left(x^2 + y^2 + z^2\right)^{\frac{1}{2}}$. The resulting potential function at point B is found, again following from Schetz and Fuhs [17], as,

$$\phi_{\sin k} = \frac{Q_{L3}}{2\pi\left(x^2 + y^2 + z^2\right)^{\frac{1}{2}}} \tag{13}$$

The first derivatives of the total potential function in Eq. (8) evaluated at point B ($x = b$, $y = h$, $z = 0$) are found as,

$$u_B = \left.\frac{\partial\phi}{\partial x}\right|_{x=b,\,y=h,\,z=0} = \frac{Q_{L2}}{hD} - \frac{Q_{L3}b}{2\pi\left(b^2 + h^2\right)^{\frac{3}{2}}} \tag{14}$$

$$v_B = \left.\frac{\partial\phi}{\partial y}\right|_{x=b,\,y=h,\,z=0} = -\frac{Q_{L3}h}{2\pi\left(b^2 + h^2\right)^{\frac{3}{2}}} \tag{15}$$

$$w_B = \left.\frac{\partial\phi}{\partial z}\right|_{x=b,\,y=h,\,z=0} = 0 \tag{16}$$

and the second derivates evaluated at point B as,

$$\left.\frac{\partial^2\phi}{\partial x\,\partial y}\right|_{x=b,\,y=h,\,z=0} = \frac{3Q_{L3}bh}{2\pi\left(b^2 + h^2\right)^{\frac{5}{2}}} \tag{17}$$

$$\left.\frac{\partial^2\phi}{\partial y^2}\right|_{x=b,\,y=h,\,z=0} = \frac{3Q_{L3}h^2}{2\pi\left(b^2 + h^2\right)^{\frac{5}{2}}} - \frac{Q_{L3}}{2\pi\left(b^2 + h^2\right)^{\frac{3}{2}}} \tag{18}$$

$$\left.\frac{\partial^2\phi}{\partial y\,\partial z}\right|_{x=b,\,y=h,\,z=0} = 0 \tag{19}$$

The velocity field is symmetrical about the x-y plane, and subsequently $w_B = 0$ in Eq. (16). The derivative definitions are substituted into Eq. (10) and the resulting equation has two unknowns for any flow condition (Q_{L2}, Q_{L3}), these are the dip height, h, and dip offset distance, b. The offset distance is a result of the transverse liquid momentum forcing the dip downstream. In effect a fourth equation is needed to have the number of unknowns equal to the number of equations. The dip angle, θ_B, as shown in Fig. 1, is defined as a function of h and b as,

$$\theta_B = \tan^{-1}\left(\frac{h}{b}\right) \tag{20}$$

A criterion for the dip offset distance, b, was proposed by Bowden and Hassan [13]; however recent analysis showed it to lead to an under-prediction of the experimental dip co-ordinates. This criterion is omitted in this study, and instead three dip angles are tested in the solution based on experimental evidence (θ_B = 40, 50 and 60 degrees) [15].

With the velocity field defined at point B through the potential function, the kinetic energy at point B can be found through the length of the velocity vector at B by,

$$V_B^2 = u_B^2 + v_B^2 + w_B^2 \tag{21}$$

and substituting the first derivatives of the total potential function in Eq. (14) to (16) evaluated at point B into Eq. (21) results in,

$$V_B^2 = \left(\frac{Q_{L2}}{hD} - \frac{Q_{L3} b}{2\pi \left(b^2 + h^2\right)^{\frac{3}{2}}} \right)^2 + \left(\frac{Q_{L3} h}{2\pi \left(b^2 + h^2\right)^{\frac{3}{2}}} \right)^2 \tag{22}$$

The model to predict the onset of gas entrainment dip is defined by the system equations provided in Eq.s (10), (20) and (22) with unknowns h, b, V_B, for given flow conditions, Q_{L2}, and Q_{L3}, and dip angle, θ_B. The link between the OGE dip phenomenon and the inlet flow is provided by a statement of Bernoulli's equation in Eq. (5) with the remaining unknown being the upstream height, H_{OGE}. In practice the flow rates between the branch and run are not independently controllable and the total inlet liquid flow rate, Q_{L1}, is dependant on several factors including the channel geometry, orientation, frictional losses, and interfacial shear. In stratified co-current gas-liquid channel flow, for example, the driving forces include gravity, interfacial shear induced by the flowing gas phase, and wall shear stresses. If the interfacial and wall shear stresses are neglected, the problem becomes analogous to open channel flow. The branch flow, on the other hand, is pressure driven and can be actively controlled using a throttling device. With the branch flow constant, the run flow is found as the difference between the inlet and branch flow rates.

The splitting of the liquid stream between the inlet, branch, and run is referred to as the liquid flow distribution. The critical liquid flow distribution, defined at OGE, was determined experimentally [15].

The model solution is a two step process. In the first step the dip characteristics (position, velocity, and acceleration) are solved using the potential function developed from Eq. (8) for an imposed branch and run flow rate, and dip angle. The OGE criterion in Eq. (10) was evaluated numerically using an in-house code to scan a physically appropriate range described by,

$$0 < y < \frac{D}{2},\ \theta_B = 40^\circ, 50^\circ, 60^\circ,\ z = 0 \tag{23}$$

The upper limit of the y-coordinate, D/2, was chosen so that the point-sink radius would not interfere with the channel side wall, thereby avoiding distortion of the sink hemispherical flow area. The root of Eq. (10), the dip location, was found using an algorithm to verify that the acceleration at the given point did not exceed 1% of the gravitational value (-9.81 m/s^2). The process was repeated over a range of imposed branch and run flow rates which were physically appropriate and based on experimental evidence [15].

In the second step the dip kinetic energy and height found from the first step are coupled with the upstream kinetic energy and height in Eq. (5) to solve for the upstream height, H_{OGE}. This was done numerically whereby Eq. (5) was scanned over a physically appropriate range where,

$$h < H_{OGE} < D \tag{24}$$

An algorithm was implemented to search for roots where the kinetic energy at the dip using the potential function (Eq. 22) was within 1% of the dip kinetic energy using Eq. (5).

In the limiting case when the crossflow velocity at the dip is zero (U_B = 0) the model is representative of quasi-stagnant stratified environment within the horizontal channel. That is to say the liquid flows into the branch symmetrically from the inlet and run.

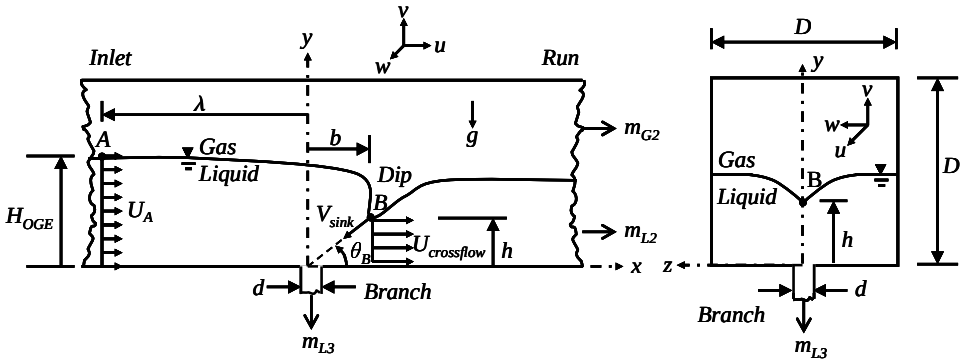

Fig. 1. Problem description

Assuming that the volume of fluid contained in the horizontal channel is sufficiently larger than the outflow of fluid through the branch, the upstream interfacial liquid velocity, point A, becomes negligible and the interface height, H_{OGE}, may be found analytically as,

$$\frac{H_{OGE}}{d} = 0.625 Fr_d^{0.4} \quad (25)$$

RESULTS AND DISCUSSION

Flow Visualization

The images presented in Fig. 2 shows the typical development of the gas entrainment flow structure in the bottom branch. In Fig. 2a the image depicts the formation of the steady dip, typical of the vortex-free gas entrainment phenomenon. In this instance the inlet liquid height and branch and run flow rates have achieved steady state. The dip structure remains relatively stable. The lowest point of the dip was found in this case to be around b = 6 mm, h = 5.9 mm, with Fr_d = 18. Reducing the inlet height, typically less than 1 mm, resulted in air entrainment into the branch, as shown in Fig 2b. Initially entrainment was observed to be transient as the dip experienced a sudden collapse into the branch and then quickly reformed. As the liquid height was decreased further, the gas phase began to steadily entrain into the branch. The visualization method used to depict the OGE does cause a bias uncertainty in the measurement of the critical height, and was estimated to be 1 mm, as it is dependant on the observer's perception of the OGE phenomenon.

The steady dip profiles obtained at branch Froude numbers of 18, 13, 11.4, and 7.9 obtained through image analysis were used to determine the dip angle, following Eq. (20).

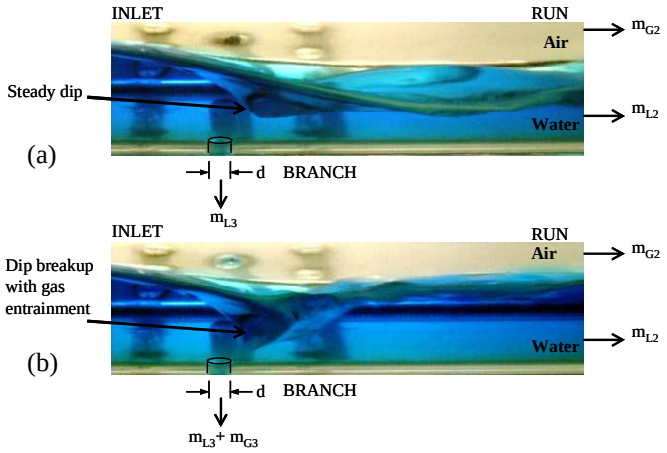

Fig. 2. Two-phase flow structure (a) just prior to gas entrainment and (b) at transient dip break-up with subsequent gas entrainment.

The number of measurements was insufficient for developing a confident relationship between the dip angle and branch Froude number. Instead, the average value was calculated over the four Froude numbers shown in Fig. 3 as,

$$\theta_B = 50^\circ, 7.9 \le \mathrm{Fr_d} \le 18 \quad (26)$$

A maximum deviation of eight degrees was found over the range of branch Froude numbers.

Critical Liquid Flow Distribution

The critical liquid flow distribution was determined by scanning the full range of allowable branch Froude numbers and recording the corresponding branch and run flow rates at OGE. The branch flow rate, Q_{L3}, is a function of the branch diameter, d, while the run flow rate, Q_{L2}, is a function of the pipe diameter, D. By dividing each of the liquid mass flow rates by the total flow areas the critical flow distribution may be represented in terms of a ratio of superficial velocities, V_{L2S}/V_{L3}. The critical flow distribution is shown in Fig. 4 and is correlated here as,

$$\frac{V_{L2S}}{V_{L3}} = 0.02 Fr_d^{-0.16}, 1 \le \mathrm{Fr_d} \le 30 \quad (27)$$

Multiplying Eq. (27) by the ratio D^2/d^2 yields the ratio of flow rates, Q_{L2}/Q_{L3}.

The total inlet mass flow rate, Q_{L1}, was observed to vary proportionally with the inlet height, and this observation was collaborated by Reimann and Khan [10]. They presented the inlet liquid mass flow rate at the maximum and minimum liquid heights, and based on this, the critical distribution was estimated from their measurements. Since they investigated two different branch diameters, 6 mm and 12 mm, respectively, the effect of d/D could be presented more readily. The critical flow distribution extracted from Reimann and Khan [10]'s results are also presented in Fig. 10. Decreasing d/D leads to a decrease in the ratio V_{L2S}/V_{L3}. This is expected since a smaller branch diameter requires less liquid flow rate to achieve the same branch Froude number.

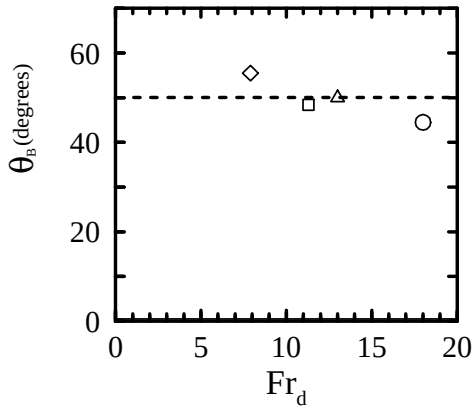

Fig. 3. Experimental dip angle.

Model Prediction

Using Eq. (27) as an empirical boundary condition, the onset of gas entrainment criterion in Eq. (10) is used to determine the dip height, h by scanning three dip angles, θ_B = 40, 50 and 60 degrees. Scanning Eq. (10) for a single branch Froude number, and over a range of heights, y, as shown in Fig. 5a, a single root is found where the acceleration is equivalent to gravity, for each dip angle. For example, for a branch Froude number of Fr_d = 15, and a dip angle of 50 degrees, the predicted dip height corresponds to h = 4.9 *mm*. Increasing the dip angle is shown to increase the predicted dip height. This can be explained through the acceleration field presented in Fig. 5b for Fr_d = 15, θ_B = 50, and h = 4.9 *mm*. The acceleration field equivalent to gravity (g = -9.81 m/s^2) is represented by a contour surrounding the branch origin (x = 0, y = 0, z = 0). The acceleration field is asymmetrical about the x-axis due to the imposed crossflow velocity from Eq. (12). In effect, the dip criterion is satisfied anywhere along this contour. Experiments have shown that for the imposed flow rates the dip angle can be expected to be in the neighborhood of 50 degrees. The dip angle, coupled with the onset criterion of Eq. (10), is necessary to determine the dip height.

The locus of dip heights, as a function of the branch Froude number and dip angle, is presented in Fig. 6a. The analytical prediction of h is compared in the figure with those obtained experimentally. The results show that h is well predicted between dip angles of 50 and 60 degrees. In this range of dip height ($0.1 < h/D < 0.13$) the difference in lateral flow area (z-direction) between a channel with a square or circular cross-section (diameter D) is on the order of 50%. It could be expected that for any given Q_{L2} the crossflow velocity, U_B, should be higher in the cylindrical channel geometry for any given dip height h. However, the impact on the sink potential function can not be overlooked. With a cylindrical channel the sink flow area is no longer hemispherical, but rather found as the intersection of a sphere and cylinder [9]. In effect the sink flow area for a circular cross-section is reduced when compared to the square channel for the same dip height h. For the same branch flow rate, the sink velocity at any radial location is therefore expected to be higher in the cylindrical channel. One could therefore speculate that the predicted dip height should be higher, if the crossflow velocity is also assumed uniform, in the case of a cylindrical channel. The effect of the channel geometry should therefore be investigated further in order to quantify its effects on the dip prediction.

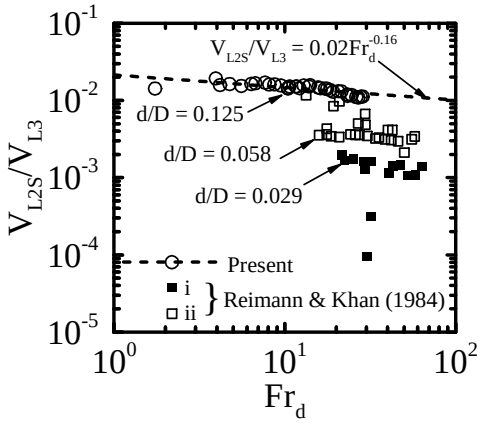

Fig. 4. Critical liquid flow distribution between run and branch.

The predicted dip crossflow Froude number, Fr_{UB}, is presented in Fig. 6b as a function of the dip height. The dip crossflow Froude number is defined as,

$$Fr_{UB} = \frac{Q_{L2}}{\left(h^3 D^2 g\right)^{\frac{1}{2}}} \tag{28}$$

which is used extensively in the study of open channel flows [18]. The crossflow Froude number reveals three distinct types of well known flow regimes in open channel flow:

- $Fr_U = 1$ Critical flow
- $Fr_U < 1$ Subcritical flow
- $Fr_U > 1$ Supercritical flow

(a)

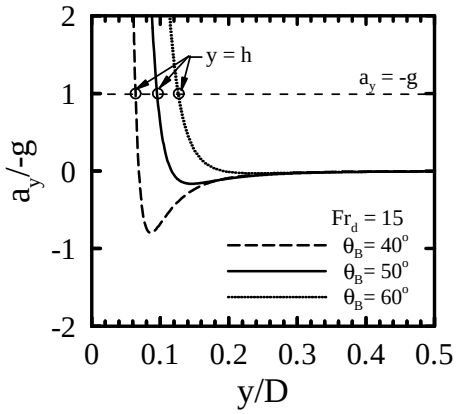

(b)

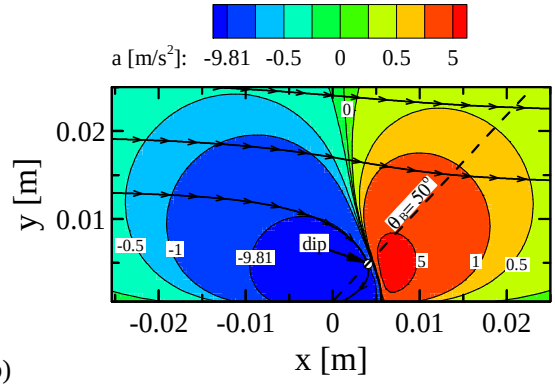

Fig. 5. Dip prediction showing (a) the critical dip height accompanied by the (b) acceleration field for Fr_d = 15 and 50 degree dip angle.

For a dip angle of 50 degrees and $h/D > 0.05$, the flow regime is shown to be supercritical, while the same regime is found for the 60 degree dip angle and $h/D > 0.1$. Interestingly, experiments showed a secondary phenomenon whereby a steady liquid jet emanated from the dip, flowing in the direction of the run. This phenomenon is shown in Fig. 2a, just to the right of the dip. When air entrained into the branch the phenomenon was dissipated, as shown in Fig. 2b. One possible explanation for this phenomenon is that the run flow becomes supercritical at the dip and produces a type of hydraulic jump.

The character of Eq. (5) as a function of the upstream height, H, is shown in Fig. 7a. The figure presents the predicted dip kinetic energy from Eq. (5) and from the potential field in Eq. (22). In the case of a large stagnant reservoir, a comparison of kinetic energies between the dip and static interface was used to predict the critical height [19]. The critical height being the vertical distance from the branch to the static interface, which follows from Craya [20]'s original analysis. The critical height is then found as a single root where the dip kinetic energy obtained from the statement of Bernoulli's equation and the potential field are equal, with Eq.s (5) and (22) being tangent to each other at the root ($U_A = U_B = 0$). The same methodology was employed in this study; however, no root was found when the upstream velocity was non-zero, as seen in the figure.

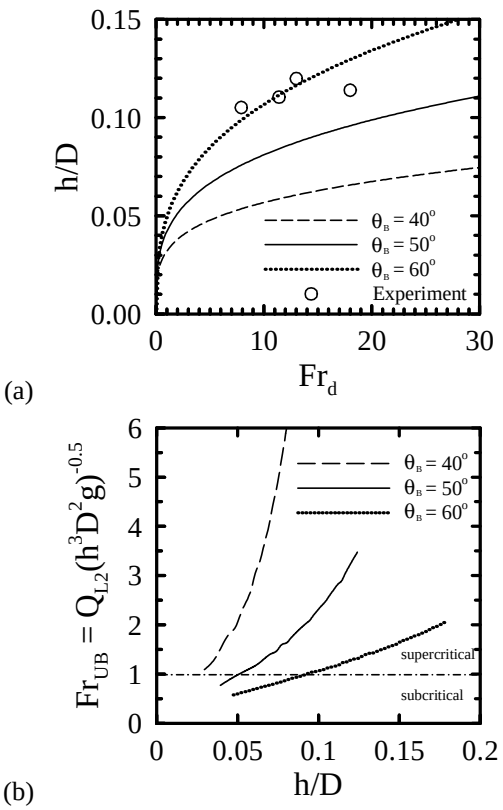

Fig. 6. (a) The predicted dip height and (b) the predicted dip crossflow Froude number.

The upstream velocity, U_A, is presented using the upstream crossflow Froude number, Fr_{UA},

$$Fr_{UA} = \frac{(Q_{L2} + Q_{L3})}{(H^3 D^2 g)^{\frac{1}{2}}} \tag{29}$$

The upstream velocity is imposed in Eq. (5) implicitly as a function of the upstream height, using Eq. (4). The consequence is that the upstream velocity term is dominant in Eq. (5) at low values of H ($H/D < 0.25$), and becomes less significant as H increases ($H/D > 0.25$). The effect is seen in the figure as Eq. (5) decreases to a minimum value at H_{crit} ($H/D = 0.25$) This minimum peak value is significant from a physical standpoint in that it represents the transition from subcritical to supercritical flow regimes as evidenced by the value of Fr_{UA}.

If the functional relationship between the upstream height and velocity are relaxed in Eq. (5), that is the upstream velocity is imposed explicitly rather than as an implicit function of H_{OGE}, a solution can be found in the form of a single root at H_{OGE}, as shown in Fig. 7b. The difference between Fig. 7a and 7b is that the upstream velocity, U_A, is set constant at 0.24 m/s in the latter. This value was not chosen haphazardly, but rather based on experimental evidence, and results in a subcritical crossflow Froude number.

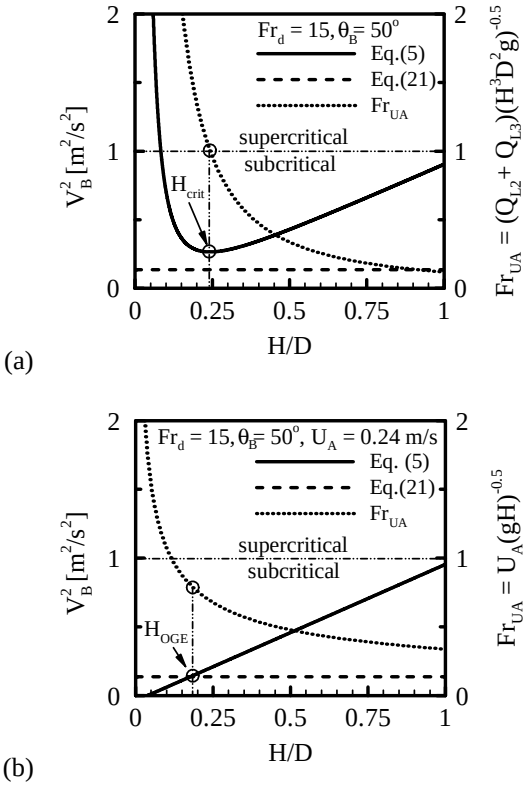

Fig. 7. Comparing the dip kinetic energy obtained from Bernoulli's equation and the potential function for (a) the inlet velocity defined as a function of the inlet height and (b) the inlet velocity defined explicitly ($U_A = 0.24$ m/s).

In order to find a solution to Eq. (5) an empirical function for the average upstream velocity was developed from the recorded values of the upstream height and flow rate as,

$$U_A = \frac{Q_{L2} + Q_{L3}}{R^2 \cos^{-1}\left(\frac{R-H}{R}\right) - (R-H)\sqrt{2RH - H^2}} \qquad (30)$$

The denominator in Eq. (30) is the lateral flow area represented by a circular segment of height H and radius R, where $R = D/2$ [21]. The value of the upstream height was taken at a distance of $\lambda / D = -5$. The resulting average velocity is shown in Fig. 8a as a function of Fr_d and was found to be best fit by,

$$U_A = 0.1 Fr_d^{0.32},\ 1 < Fr_d < 30 \qquad (31)$$

Over the range of H the flow is subcritical with Fr_U ranging between 0.4 and 0.6, as shown from Fig. 8b. The resulting locus of solutions for the upstream heights, as a function of Fr_d, is presented in Fig. 8c and is shown in comparison to the experimental upstream height. The upstream height is not well predicted over the three dip angles tested, and the error is on the order of approximately 50% for a dip angle of 50 degrees. Several factors contribute to this error, including the omission of energy changes due to shear and inertial effects in Eq. (5). The interfacial liquid gradient in horizontal channels with co-current gas-liquid flow has been shown to be well predicted when wall friction and interfacial shearing are considered [22]. Secondly, the interfacial velocities are likely not well represented by the average velocity, particularly in the near branch region. Lastly, the channel geometry impacts the dip prediction, which in turn, will affect the upstream height prediction.

CONCLUDING REMARKS

Experiments have shown that the stratified flow is hydrodynamically developing upstream of the branch, within the inlet region. This results in an interfacial liquid gradient within the inlet region, and consequently, a single unique critical height to characterize the onset of gas entrainment phenomenon is un-realistic. This is in contrast to the stagnant reservoir case where a single critical height is reasonable. Experiments also showed that the dip structure is dependant on the imposed flow conditions. The dip angle was recorded over a limited range of Froude numbers in this study, and was assumed to have a constant value. In reality, this is not the case, as the dip position, size, and orientation are expected to be influenced by the ratio of momentum fluxes between the run and branch flows.

The analytical model was shown to predict the dip height for the applied flow conditions well; however the inlet height could not be predicted without an empirical function to describe the inlet velocity. The dip and inlet region were coupled through Bernoulli's equation and consequently the effects of wall and interfacial shear, as well as inertial effects due to the velocity profile development, were neglected.
Future directions include,

- Using circular inlet/run pipe geometry to improve the geometric representation of the problem.
- Simulation of the flow field using a finite diameter branch rather than a point-sink.
- Investigating shear and inertial effects between the dip and inlet regions.
- Developing an analytical criterion for the dip angle.

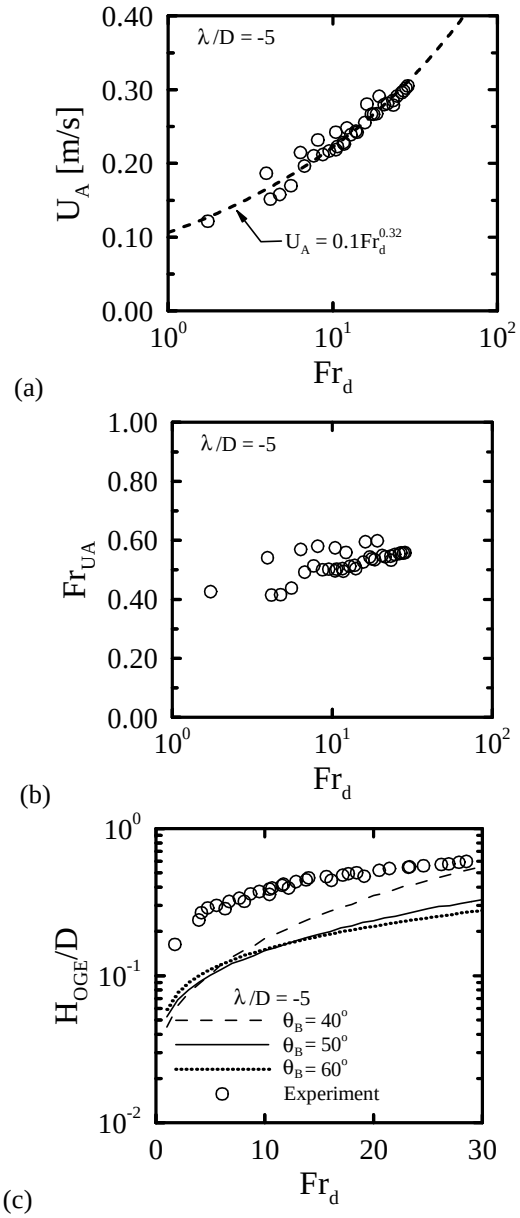

Figure 8. (a) The inlet average velocity accompanied by (b) the inlet crossflow Froude number and (c) inlet height prediction compared with experiments.

ACKNOWLEDGEMENTS

Financial support provided by the Natural Sciences and Engineering Research Council of Canada (NSERC), the Alexander Graham Bell Post-graduate scholarship program, the Hydro-Quebec scholarship program, and the Canada Foundation for Innovation (CFI) are gratefully acknowledged.

REFERENCES

[1] Azzopardi, B.J., 1999, "Phase Separation at T Junctions", *Muliphase Science and Technology*, **11**, 223-329.

[2] El-Shaboury, A.M.F., Soliman, H.M., Sims, G.E., 2007, "Two-phase Flow in a Horizontal Equal-Sided Impacting Tee Junction", *International Journal of Multiphase Flow*, **33**, 411-431.

[3] Margaris, D.P., 2007, "T-Junction Separation Modelling in Gas-Liquid Two-Phase Flow", *Chemical Engineering and Processing*, **46**, 150-158.

[4] Hardy, P.G., Richter, H.J., 1987, "Small break loss of coolant accidents: bottom and side break", *Nuclear Engineering and Design*, **100**, 75 – 86.

[5] Kowalski, J.E., Krishnan, V.S., 1987, "Two-phase Flow Distribution in a Large Manifold", *Proceedings of the AIChE Annual Meeting*, New York, NY.

[6] Ardron, K.H., Bryce, W.M., 1990, "Assessment of Horizonatal Stratification Entrainment Model in RELAP5/MOD2 by comparison with Separate Effects Experiments" *Nuclear Engineering and Design*, **122**, 263-271.

[7] Zuber, N., 1980, "Problems in Modeling of Small Break LOCA", *Nuclear Regulatory Commission Report*, **NUREG-0724**.

[8] Ahmad, T., Hassan, I., 2006, "Experimental Investigation on the Onset of Gas Entrainment from a Stratified Two-phase region through Multiple Branches Mounted on a Curved Surface", *J. Fluids Engineering, ASME*, **128**, 726-733.

[9] Saleh, W., Bowden, R.C., Hassan, I.G., Kadem, L., 2009, "A Hybrid Model to Predict the Onset of Gas Entrainment With Surface Tension Effects", *J. Fluids Engineering, ASME*, **131**, 011305-011315.

[10] Reimann, J., Khan, M., 1984, "Flow through a Small Break at the Bottom of a Large Pipe with Stratified Flow", *Nuclear Science and Engineering*, **88**, 297-310.

[11] Smoglie, C., Reimann, J., 1986, "Two-phase Flow Through Small Branches in a Horizontal Pipe with Stratified Flow", *Int. J. Multiphase Flow*, **12**, 609-625.

[12] Maciaszek, T., Micaelli, J.C., 1990, "CATHARE Phase Separation Modeling for Small Breaks in Horizontal Pipes with Stratified Flow" *Nuclear Engineering and Design*, **124**, 247-256.

[13] Bowden, R.C., Hassan, I.G., 2009, "Modeling the Onset of Gas Entrainment in a Single Downward Discharge From a Stratified Gas-Liquid Region with Liquid Crossflow", *J. Fluids Engineering, ASME*, **131**, 031304-1 – 031304-8.

[14] Andaleeb A., Hassan, I., Saleh, W., Ahmad, I., 2006, "Modeling the Onset of Gas Entrainment from a Stratified Two-Phase Region Through Branches on a Curved Surface", *J. Fluids Engineering, ASME*, **128**, 717 – 725.

[15] Hassan, I., Bowden, R., Saleh, W., 2009, "Co-current Stratified Gas Liquid Flow in a Horizontal Pipe with A Discharging Branch" *Proceedings in 7th Conference on Nuclear and Particle Physics, NUPPAC'09*, Sharm El-Sheikh, Egypt, 11-15 Nov. 2009.

[16] White, F.M., 1991, "Viscous Fluid Flow", *McGraw-Hill*, New York.

[17] Schetz, J. A., Fuhs, A. E., 1996, "Handbook of Fluid Dynamics and Fluid Machinery", *Fundamentals of Fluid Mechanics*, **Vol. 1**, Wiley, New York.

[18] Chow, V.T., 1959, "Open Channel Hydraulics", *McGraw-Hill*, New York.

[19] Soliman, H.M., Sims, G.E., 1992, "Theoretical Analysis of the Onset of Liquid Entrainment for Orifices of Finite Diameter", *Int. J. Multiphase Flow*, **18**, 229-235.

[20] Craya, A., 1949 "Theoretical Research on the Flow of Nonhomogeneous Fluids", *La Houille Blanche*, **4**, 44-55.

[21] Zwillinger, D., 1996, "Standard Mathematical Tables and Formulae", 30th ed., CRC Press, Boca Raton, Florida.

[22] Sadatomi, M., Kawaji, M., Lorencez, C.M., Chang, T., 1993, "Prediction of Liquid Level Distribution in Horizontal Gas-Liquid Stratified Flows with Interfacial Level Gradient", *International Journal Multiphase Flow*, **19**, 987 – 997.